ACS APPLIED MATERIALS & INTERFACES

Research Article

www.acsami.org

Liquid-Phase-Deposited Silicon Oxide Film as a Mask for Single-Sided Texturing of Monocrystalline Si Wafers

Tao Lin,[†] Kun Jiang,[†] Bo-Xuan Zhou,[‡] Su-Fan Xu,[‡] and Wen-Bin Cai*[,†]

[†]Shanghai Key Laboratory of Molecular Catalysis and Innovative Materials, Collaborative Innovation Center of Chemistry for Energy Materials, Department of Chemistry, Fudan University, Shanghai 200433, China

[‡]RENA (Shanghai) Co., Ltd., 1155 Fang Dian Road, Shanghai 201204, China

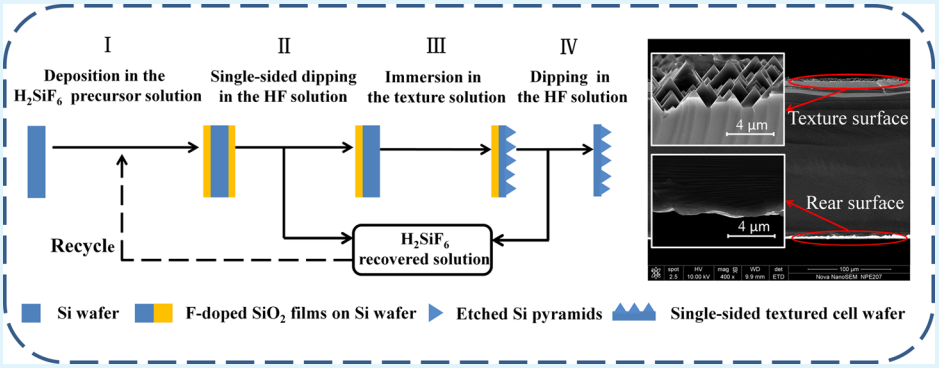

ABSTRACT: A silicon oxide film doped with fluorine was grown on a (100)-oriented Si wafer through liquid-phase deposition (LPD) as a protective mask of the wafer's rear side in order to chemically texture the wafer's unprotected front side in a basic etching bath, which is a new process in solar-cell manufacturing. The growth rate of the LPD-SiO_2 film increased monotonically with an increase of the deposition temperature up to 60 °C for a given precursor solution. Field-emission scanning electron microscopy (FE-SEM) indicates that a pyramidal surface texture forms on the front side in the chemical texturing bath, whereas the underlying Si surface on the rear side remains intact. As a result, the average reflectivity for incident light over 450−850 nm is decreased to 11.1% on the front side, and a 5.8 μm thick Si surface on the rear side is saved per wafer. The all-wet process involved in this single-sided texturing is promising for the mass production of thinner and higher-efficiency Si-based solar cells because of its simplicity and lower cost.

KEYWORDS: *liquid-phase deposition, silicon oxide film, silicon wafer, single-sided texturing, solar cells*

1. INTRODUCTION

Saving on the cost of monocrystalline Si wafers and increasing the photoelectric conversion efficiency are two key issues facing the development of Si-based solar cells.[1−5] Along this line, reducing the thickness of solar-cell wafers without compromising their performance is always pursued in mass-scale production. To obtain a higher light-trapping performance for solar cells, surface texturing of Si wafers is indispensable because it helps to increase the optical path length and to reduce the incident light reflection. Nowadays, double-sided texturing in alkaline etchants is widely used in the manufacture of monocrystalline Si wafer-based solar cells.[6−8] This process removes a dozen or even dozens of micrometers thick Si layer, which may hamper the increasing demand for a lower usage of Si in solar-cell production because the further wafer thickness reduction increases the crash ratio and the mechanical yield losses of the modules in the follow-up screen-printing (SP) of the so-called aluminum back-surface field (Al-BSF) film.[1,5] In addition, the rear-surface recombination of photoinduced carriers could be exacerbated for an over-reduced cell wafer thickness, leading to a decreased short-circuit current,[3] thus posing a technical challenge for the formation of a more critical Al-BSF to achieve a higher passivation effect.

To address the issue caused by double-sided texturing, single-sided texturing has been attempted in which the rear side of the Si wafer is either kept away from the etchant solution or coated with a mask. The former has been achieved by floating Si wafers across the liquid level of a texturing solution through conveyor rollers with their back surfaces exposed to the air.[9] For the latter, a plasma-enhanced chemical deposition (PECVD)-deposited SiN_x film has been utilized as a mask layer on the rear surface of Si wafer.[10,11] Obviously, single-sided texturing prevents the undesired dissolution of Si monocrystalline wafers, enabling the use of thinner pristine Si wafers in the manufacture of solar cells and thus saving on the production cost. In addition, the Al-BSF layer covering on a relatively flat rear surface from single-sided texturing provides an improved uniformity of the Al−Si alloy formation, advanced passivation

Received: November 5, 2013
Accepted: December 27, 2013
Published: December 27, 2013

Scheme 1. Schematic Representation of the Wet-Chemical Single-Sided Texturing Process

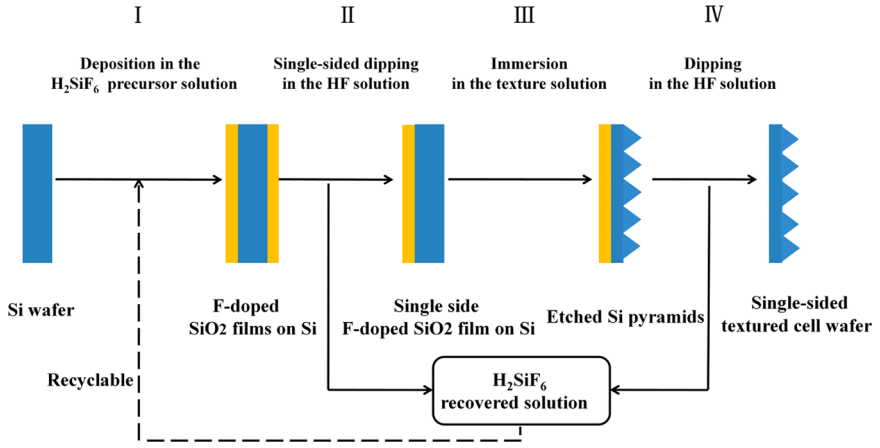

effect, and superior cell performance as compared to the same covering on a rough back surface from double-sided texturing.[4,10] Unfortunately, the single-sided texturing processes reported so far either require a longer length of equipment and increased consumption of the texturing solution because of its evaporation at 70−90 °C (for the conveyor-roller-driven wafer-floating method) or have to be handled in vacuum with expensive equipment and complex operations (for the PECVD method), calling for urgent research on alternative cost-effective single-sided texturing methods.

A wet-chemistry process has been widely applied to surface cleaning, modification, and deposition on Si substrates[12−15] owing to its facile and cost-effective advantages. Specifically, since the pioneering work on liquid-phase deposition (LPD) by Kawahara et al.,[16] this wet-chemistry process has been widely used to grow various functional coatings including SiO_2, TiO_2, and other metal-oxide films for applications in microelectronics, photocatalysis, dye-sensitized solar cells, and chemical sensing.[17−20] The LPD method possesses distinguishing advantages such as low temperature, high selectivity, large area, simplicity, and support of mass production.[20,21]

In this study, we extend the LPD method to grow a fluorine-doped SiO_2 film on monocrystalline Si wafers and initially explore the new application of this film as a sacrificial mask against corrosive etching of the underlying Si in basic texturing solutions. The present work opens an avenue for a new single-sided texturing process in the mass production of monocrystalline Si-based solar cells.

2. EXPERIMENTAL SECTION

2.1. Liquid-Phase Deposition of SiO_2. A p-type unpolished Si (100) wafer, with a thickness of 190 ± 10 μm and a resistivity of 1−3 Ω cm, was cut into dimensions of 2.6 × 2.6 cm^2 by a laser. It was then sequentially subjected to standard RCA 1 ($H_2O/NH_3{\cdot}H_2O/H_2O_2$ = 5:1:1) and RCA 2 ($H_2O/HCl/H_2O_2$ = 6:1:1) cleaning procedures to degrease and remove the metal ions and organic impurities from the surface. The OH-terminated Si surface thereby formed also facilitated the LPD process afterward. To prepare the precursor solution, an excessive amount of silicic acid in powder form ($SiO_2{\cdot}xH_2O$) was added to a 35 wt % hydrofluorosilicic acid (H_2SiF_6) aqueous solution, the mixture was stirred for over 3 h at room temperature, and the undissolved silicic acid powder was removed by filtration. The filtered saturated H_2SiF_6 solution was diluted with deionized (DI) water and a boric acid aqueous solution to a concentration of 2 M, with the concentration of boric acid adjusted to 0.5 mM. After a thorough rinse with DI water and drying, the RCA-cleaned Si wafer was immersed vertically in the precursor solution, and the deposition temperature was set at 40, 50, 60, or 70 °C under stirring. At a desired deposition time, the substrate was removed from the solution, thoroughly rinsed with DI water under sonication, and dried under nitrogen flow.

2.2. Single-Sided Texturing Process. The entire process included four main steps for the creation of {111}-preferred pyramids on the front side of a Si (100) wafer, as shown in Scheme 1 and detailed as follows:

(I) Si (100) wafers were covered with a film of LPD-deposited SiO_2, front and back, to act as an etch barrier. The details of this step were described earlier.

(II) The SiO_2 film on the front side was removed by dispersing aliquots of 5% HF solution on the surface and allowing the reaction to proceed for 1 min at room temperature followed by a thorough rinse with Milli-Q water.

(III) The Si wafer was dipped into a 1.25 wt % KOH aqueous solution at 75 °C for 2 min to accomplish the rough-polishing process. Then, it was cleaned in a mixture of 1.62 wt % KOH and 4.7 vol % H_2O_2 at 75 °C for 3 min. Next, the rough-polished and cleaned Si wafer was perpendicularly immersed in the texturing solution consisting of 2 wt % KOH, 2.3 vol % RENA Mono Tex M type, and 0.45 vol % Mono Tex D type surfactants at 75 °C for 12 min.

(IV) The SiO_2 coating layer on the back side of the Si wafer was removed by soaking in 5% HF.

2.3. Measurement and Characterization. The thickness of a LPD film was measured by an automated film-thickness mapping system (F50, Filmetrics, USA). The chemical bonding and structure of the as-deposited SiO_2 film was investigated using a Fourier transform infrared spectrometer (Nicolet is50, Thermo Scientific, USA) in the transmission mode by using the undeposited Si area as the background. A field-emission scanning electron microscope (Nova NanoSEM 450 with TLD-detector, FEI, USA) was utilized to characterize the structural morphology of the LPD film and textured surface. A diffusion 8° integration sphere 8° spectroscopic reflectometer (Raditech, Taiwan) consisting of a xenon lamp with a wavelength of 220−2500 nm, an UV−NIR spectrometer, and a back thin CCD detector was used to determine the corresponding surface optical reflectance.

3. RESULTS AND DISCUSSION

3.1. Effect of Deposition Temperature. The chemical reactions for the growth of the silicon oxide film are simply proposed as follows[22]

$$H_2SiF_6 + 2H_2O \leftrightarrow 6HF + 2SiO_2, \quad \Delta H > 0 \tag{1}$$

$$H_3BO_3 + 4HF \leftrightarrow BF_4^- + H_3O^+ + 2H_2O \tag{2}$$

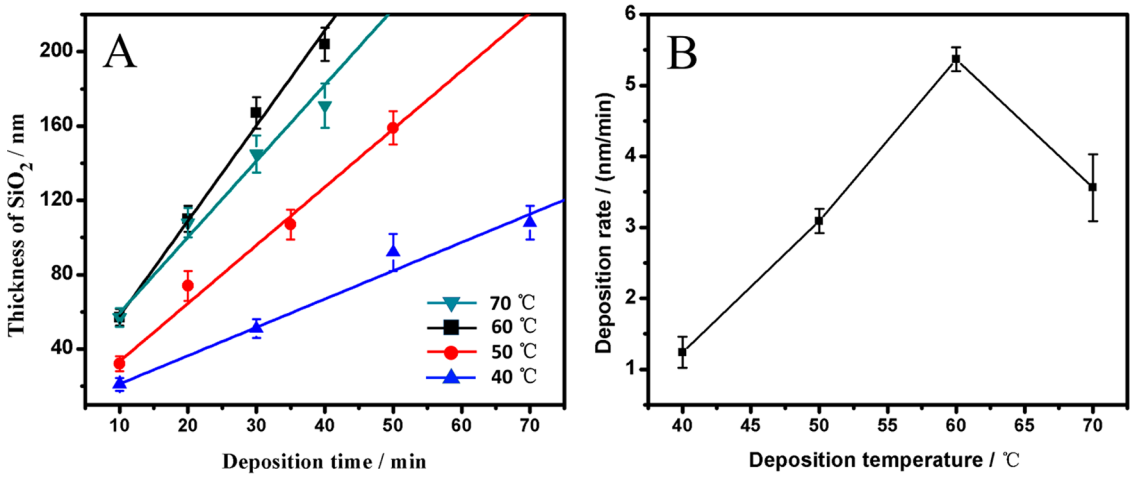

Figure 1. (A) Dependence of LPD-SiO_2 film thickness on the deposition time under varying temperatures. (B) Deposition rate of the LPD-SiO_2 film on Si substrate as a function of deposition temperature. The deposition bath contains 2 M H_2SiF_6 and 5 mM H_3BO_3.

The liquid deposition of SiO_2 results from the broken hydrolysis equilibrium between hydrofluorosilicic acid and water, as represented by eq 1. H_3BO_3 is added as the fluoride scavenger to drive eq 1 to the right, which not only prompts SiO_2 deposition but also prevents the accumulated HF from dissolving the as-formed SiO_2, as shown by eq 2. Notably, OH-terminated Si surfaces (owing to the above RCA pretreatment) or the initial ultrathin native oxide film may serve as the nucleation site for further growth of the LPD SiO_2 film. Nevertheless, SiO_2 may also precipitate in the solution when the local concentration of SiO_2 is oversaturated. However, from eqs 1 and 2, the incorporation of fluoride to the SiO_2 film can be anticipated, which was indeed confirmed by the following IR spectroscopic characterization.

The deposition rate of the mask film is an important factor that should be taken in account in practice. The hydrolysis of H_2SiF_6 (eq 1) is an endothermic reaction. An increase in the temperature may drive the reaction equilibrium to the right in addition to increasing the reaction rate. Unlike in previous investigations for producing low-K dielectrics[16,23,24] where a deposition temperature lower than 60 °C was frequently adopted, here we extended the operating temperature up to 70 °C. Because the SiO_2 film is targeted for protecting the Si substrate against the basic texturing solution, it will be favorable for mass production if the deposition time can be significantly and securely shortened. Figure 1A shows the variation of the SiO_2 film thickness with the deposition time for different deposition temperatures, and Figure 1B plots the corresponding deposition rate as a function of the deposition temperature. The thicknesses in all cases increase nearly linearly with deposition time. Furthermore, a higher deposition temperature results in a higher deposition rate (i.e., 1.2, 3.0, and 5.3 nm min^{-1} at 40, 50, and 60 °C, respectively) except for a growth rate of 3.6 nm min^{-1} at 70 °C. This is largely in agreement with the endothermic nature of the hydrolysis reaction of H_2SiF_6 and the unique role of H_3BO_3. A decrease of film growth rate at 70 °C arises from a competitive aggregation and precipitation of SiO_2 in the precursor solution because of a significant loss of water as the temperature increases as well as the poor adhesiveness of the deposited film.[24] In the following section, an operating temperature of 60 °C is preferred for the growth of the LPD film on Si wafer.

3.2. Structure of the LPD Film. The morphology and microstructure of a LPD-SiO_2 film is shown in Figure 2A,B. A

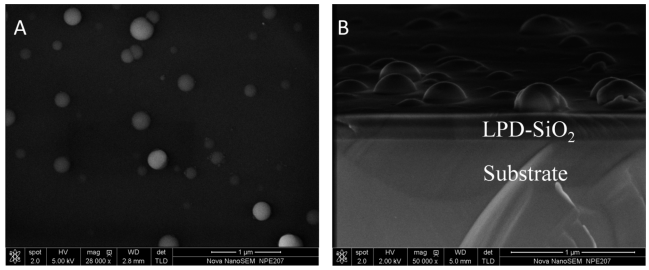

Figure 2. FE-SEM images of an LPD silicon oxide film (thickness of ca. 190 nm) deposited in a 2.0 M H_2SiF_6 solution with the addition of 5 mM H_3BO_3 at 60 °C: (A) vertical view and (B) fractured, tilted view.

densely packed film with a thickness of ca. 190 nm was observed above the Si substrate, with protruded particles of several hundred nanometers in size randomly embedded in the film. The deposition mechanism mentioned earlier could be used to explain the morphology and microstructure of the film: the hydrolysis of the H_2SiF_6 precursor with a high degree of supersaturation promoted a homogeneous nucleation of SiO_2 in solution, and some of these colloidal particles tend to adsorb onto the dynamically growing film on the OH-terminated Si substrate, which is accompanied by packing among the adsorbed particles.[24]

Figure 3 reveals the Fourier transform infrared (FTIR) spectra of the as-deposited LPD SiO_2 films with different thicknesses: (a) 303, (b) 284, (c) 235, and (d) 191 nm. For all samples, peaks characteristic of the LPD-SiO_2 films were identified, that is, the antisymmetric stretching mode at 1095 cm^{-1}, the rocking mode at 457 cm^{-1}, and the bending mode at 804 cm^{-1} of Si−O−Si.[24−26] The relatively weak band at 930 cm^{-1}, attributable to Si−F stretching, indicates that fluorine is self-incorporated into the SiO_2 films during the LPD process.[25,26] A shoulder at 1200 cm^{-1} suggests a strengthened Si−O−Si stretching of the LPD films as compared to that of thermally formed SiO_2 films. Moreover, a frequency shift of the antisymmetric stretching mode of Si−O−Si from ca. 1080 cm^{-1} for thermally grown SiO_2 films to ca.1095 cm^{-1} for LPD-SiO_2

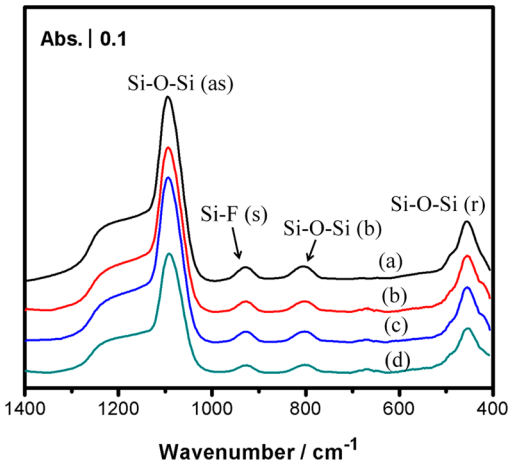

Figure 3. FTIR spectra of LPD-SiO_2 films with different thicknesses deposited at 60 °C: (a) 303, (b) 284, (c) 235, and (d) 191 nm (as, antisymmetric stretching mode; s, stretching mode; b, bending mode; and r, rocking mode).

films may be attributed to the incorporated Si−F bond that has a larger dipole moment in the latter.[25]

3.3. LPD Film as the Mask in Texturing. Anisotropic chemical etching of monocrystalline Si wafers was used to create an antireflective surface owing to the selective etching of the {100} plane to expose the {111} plane preferentially. In this work, the rear surface of a Si wafer was protected with an as-formed LPD-SiO_2 mask, whereas the front surface with the LPD-SiO_2 film that was removed by HF (step II in section 2.2) was textured according to eq 3 (given the fact that the dissolution of SiO_2 is much slower in an alkaline solution (eq 4) than that of Si). Nevertheless, on the basis of our visual inspection, the LPD-SiO_2 film should be thicker than 120 nm to keep the Si substrate securely intact. The LPD mask was then quickly removed with a subsequent immersion in a HF solution, as represented by eq 5. To be integrated into future solar-cell manufacture, front-side-textured Si wafers need to go through other regular procedures after removal of the protective mask on the rear side, including surface passivation with aluminum back-surface field (Al-BSF), to ensure efficient carrier collection.

$$Si + H_2O + OH^- \rightarrow SiO_2(OH)^{2-} + 2H_2\uparrow \quad (3)$$

$$SiO_2 + 2OH^- \rightarrow SiO_3^{2-} + H_2O \quad (4)$$

$$SiO_2 + 6HF \rightarrow SiF_6^{2-} + 2H_2O + 2H^+ \quad (5)$$

Figure 4 compares the FE-SEM micrographs (lateral view) of textured Si wafers without (A) or with (B) a 140 nm thick LPD-SiO_2 mask. As shown in Figure 4A, for bare Si, both the front and rear surfaces are etched, leading to a texture with pyramids having a height up to 4 μm. In contrast, for single-side-protected Si, it can be seen from Figure 4B that the same texture shows up on the unprotected front side (top inset) but is absent on the rear side (bottom inset).

The success of single-sided texturing with the aid of the LPD film can be further confirmed by examining FE-SEMs with vertical and tilted views of both sides of the Si wafer after the described steps depicted in Scheme 1. Figure 5A,B shows that a wide array of pyramids arranges tightly and orderly on the front surface. Complementary to Figure 4B, no pyramids can be observed on the rear surface from the vertical view, as shown in

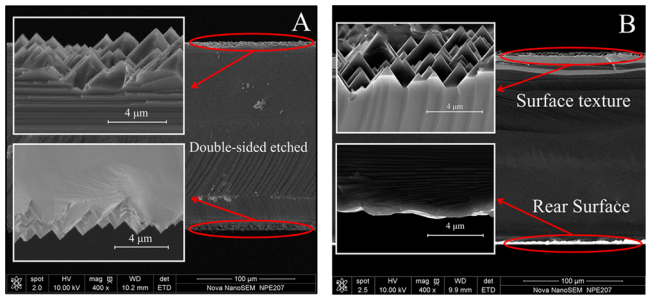

Figure 4. Selected scanning electron microscopy images from the cross section of textured Si wafers: (A) double-side-textured Si wafer and (B) single-side-textured Si wafer. The insets show the front (top) and rear (bottom) surfaces.

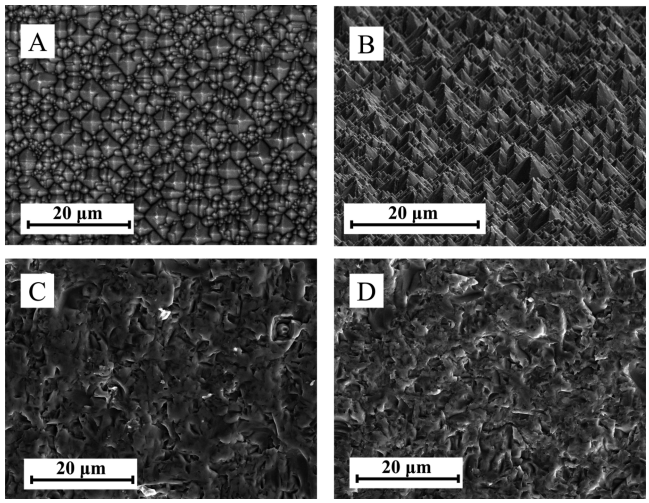

Figure 5. Vertical (A) and tilted (B) FE-SEM views of the single-side-textured wafer front surface. (C) FE-SEM image of the rear surface. (D) FE-SEM image of an untreated bare Si surface.

Figure 5C. In fact, the morphology of the rear surface of the single-side-textured Si wafer (Figure 5C) is nearly identical to that of a pristine bare Si wafer surface (Figure 5D).

3.4. Optical Reflectance and Material Loss of Textured Si Wafers. To obtain a high light-trapping performance and conversion efficiency of solar cells, a lower reflectivity of the Si wafer surface is required. The reflectivity of a double-side-textured Si wafer or an untreated bare Si wafer as a function of incident-light wavelength is shown in Figure 6A. A surface with pyramidal texture subjected to the regular double-sided texturing treatment yields a mean reflectivity of 10.6%, whereas the untreated bare Si surface gives 25.1% in the wavelength range of 450−850 nm, as listed in Table 1. The significant decline in reflectivity is due to the contiguous bipyramidal texture exposed preferentially with {111} planes.[7,27] When light hits the surface normally, it experiences multiple reflections and refractions at local pyramidal facets, leading to significantly enhanced absorption of light accompanied by significantly decreased reflection compared to the light incidence at a regular, untreated Si-wafer surface.[27,28]

Notably, the single-side-textured front surface has a reflectance close to the above-mentioned surface resulting from a conventional double-sided texturing process, giving rise to a mean reflectivity value of 11.1% in the wavelength range of 450−850 nm (Table 1). Meanwhile, the LPD-SiO_2-film-protected rear surface with the texturing treatment and the

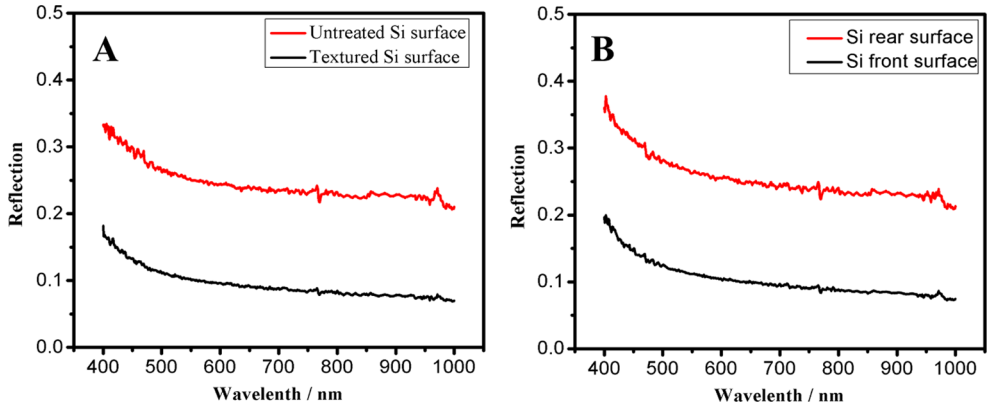

Figure 6. Optical reflectance of various Si wafer surfaces: (A) double-side-textured Si surface (black curve) and untreated bare Si-wafer surface (red curve) and (B) front surface (black curve) and rear surface (red curve) of single-side-textured Si wafer.

Table 1. Summary of the Optical Property and Material Loss of Different Si Wafers

	double-side-etched Si wafer	bare Si wafer (untreated)	single-side-textured Si wafer (front surface)	single-side-textured Si wafer (rear surface)
reflectivity	10.6 ± 0.4%	25.1 ± 0.4%	11.1 ± 0.2%	25.6 ± 0.6%
thickness loss of Si wafer/ μm	11.2 ± 1.2		5.4 ± 0.6	

subsequent removal of the mask also demonstrates a mean reflectivity (25.6%) that is the same (within measurement error) as that of a pristine Si-wafer surface (Figure 6B and Table 1). Furthermore, the results confirm that the new single-sided texturing process shown in Scheme 1 did not compromise the antireflective performance of the textured front side of a Si wafer, whereas the rear side was effectively protected. The lower reflectivity value around 11.1% for a single-side-textured surface meets the industrial standard. The optical property observed here agrees with the above morphological characterization seen in Figure 6.

The thickness losses of two types of textured Si wafers were calculated according to eq 6

$$\Delta T = \frac{\Delta m}{A\rho_{Si}} \quad (6)$$

where ΔT is the thickness loss of a wafer, Δm is the wafer mass loss because of texturing, A is defined by the length times the width of the wafer, and ρ_{Si} is the solid density of Si with a reference value of 2.33 g cm^{-3}. The method to acquire textured-wafer thickness loss is commonly used in the high-purity Si-wafer-based solar-cell industry. As shown in Table 1, the wafer thickness loss for the single-sided texturing is 5.4 μm, which is half of that for the double-sided texturing (11.2 μm), demonstrating that our designed texturing process can effectively save the thickness (and the cost) of a pristine monocrystalline Si wafer. Compared to the high-purity monocrystalline Si material, H_2SiF_6 is a relatively inexpensive Si source. Using the LPD-SiO_2 film as a protective mask in the single-sided texturing process reduces the loss of a crystalline Si wafer by half. Moreover, the recyclability of the Si source through a circulation route demonstrated in Scheme 1 and eq 5 promises a further reduction of the cost in practice.

4. CONCLUSIONS

Liquid-phase deposition was extended to grow a F-doped Si oxide film on solar-cell-oriented Si wafer to serve as the protective mask of the rear side of the Si to texture the front side of the Si in an alkaline-etchant solution. A rather high growth rate of 5.3 nm min^{-1} was achieved at a deposition temperature of 60 °C. Single-sided texturing of a Si wafer with its rear surface coated with a 120 nm (and greater) thick LPD film has enabled the reflectivity of its front surface to be reduced to 11.1% while an essentially intact rear Si side is maintained. Furthermore, compared to the conventional double-sided texturing, the thickness loss of the Si wafer was reduced by half (i.e., 5.4 vs 11.2 μm per piece). This all-wet circulatory single-sided texturing process, aiming to save Si material and to improve the photoelectric conversion efficiency, is promising for integration into the mass production of Si-wafer-based solar cells.

AUTHOR INFORMATION

Corresponding Author

*E-mail: wbcai@fudan.edu.cn.

Notes

The authors declare no competing financial interest.

ACKNOWLEDGMENTS

This work was supported by RENA Co. Ltd, NSFC (nos. 21073045 and 21273046), and SMCST (nos. 11JC140200 and 08DZ2270500). We appreciate Dr. Qiao-Xia Li for her technical help in revising the manuscript.

REFERENCES

(1) Gu, X.; Yu, X. G.; Xu, J. L.; Fan, R. X.; Yang, D. R. *Prog. Photovoltaics* **2013**, *21*, 456−461.
(2) Petermann, J. H.; Zielke, D.; Schmidt, J.; Haase, F.; Rojas, E. G.; Brendel, R. *Prog. Photovoltaics* **2012**, *20*, 1−5.
(3) Tool, C.; Burgers, A.; Manshanden, P.; Weeber, A.; Van Straaten, B. *Prog. Photovoltaics* **2002**, *10*, 279−291.
(4) Hartley, O. N.; Russell, R.; Heasman, K. C.; Mason, N. B.; Bruton, T. M. Proceedings of the 29th IEEE Photovoltaics Specialists Conference, New Orleans, LA, May 19−24, **2002**.
(5) Duerinckx, F.; Szlufcik, J. *Sol. Energy Mater. Sol. Cells* **2002**, *72*, 231−246.

(6) Seidel, H.; Csepregi, L.; Heuberger, A.; Baumgartel, H. *J. Electrochem. Soc.* **1990**, *137*, 3626−3632.
(7) Vazsonyi, E.; De Clercq, K.; Einhaus, R.; Van Kerschaver, E.; Said, K.; Poortmans, J.; Szlufcik, J.; Nijs, J. *Sol. Energy Mater. Sol. Cells* **1999**, *57*, 179−188.
(8) Marrero, N.; Gonzalez-Diaz, B.; Guerrero-Lemus, R.; Borchert, D.; Hernandez-Rodriguez, C. *Sol. Energy Mater. Sol. Cells* **2007**, *91*, 1943−1947.
(9) Mueller, G. G.; McMullen, B. Single-Sided Textured Sheet Wafer. U.S. Patent Appl. 12/546,942, Aug 25, 2009.
(10) Guo, A. J.; Ye, F. M.; Guo, L. H.; Ji, D.; Feng, S. M. *Chin. J. Semicond.* **2009**, 48−50.
(11) Thorstensen, J.; Foss, S. E.; Gjessing, J. *Prog. Photovoltaics* [Online early access]. DOI: 10.1002/pip.2335. Published Online: Jan 16, **2013**.
(12) Huo, S. J.; Xue, X. K.; Li, Q. X.; Xu, S. F.; Cai, W. B. *J. Phys. Chem. B* **2006**, *110*, 25721−25728.
(13) Wang, X. C.; Cai, W. B.; Wang, W. J.; Liu, H. T.; Yu, Z. Z. *Surf. Coat. Technol.* **2003**, *168*, 300−306.
(14) Yang, Y. Y.; Zhang, H. X.; Cai, W. B. *J. Electrochem.* **2013**, *19*, 6−16.
(15) Miyake, H.; Ye, S.; Osawa, M. *Electrochem. Commun.* **2002**, *4*, 973−977.
(16) Nagayama, H.; Honda, H.; Kawahara, H. *J. Electrochem. Soc.* **1988**, *135*, 2013−2016.
(17) Gouzman, I.; Girshevitz, O.; Grossman, E.; Eliaz, N.; Sukenik, C. N. *ACS Appl. Mater. Interfaces* **2010**, *2*, 1835−1843.
(18) Dadgostar, S.; Tajabadi, F.; Taghavinia, N. *ACS Appl. Mater. Interfaces* **2012**, *4*, 2964−2968.
(19) Yu, Q. W.; Feng, Y. Q. *Prog. Chem.* **2011**, *23*, 1211−1223.
(20) Huang, J. J.; Lee, Y. T. *Surf. Coat. Technol.* **2013**, *231*, 257−260.
(21) Iizuka, S.; Ooka, S.; Nakata, A.; Mizuhata, M.; Deki, S. *Electrochim. Acta* **2005**, *51*, 802−808.
(22) Lee, M. K.; Ho, C. L.; Zeng, J. Y. *Phys. Status Solidi A* **2008**, *205*, 231−234.
(23) Chou, J. S.; Lee, S. C. *J. Electrochem. Soc.* **1994**, *141*, 3214−3218.
(24) Yu, S. J.; Lee, J. S.; Nozaki, S.; Cho, J. H. *Thin Solid Films* **2012**, *520*, 1718−1723.
(25) Yeh, C. F.; Chen, C. L. *J. Electrochem. Soc.* **1995**, *142*, 3579−3583.
(26) Wei, J. H.; Lee, S. C. *J. Electrochem. Soc.* **1997**, *144*, 1870−1874.
(27) Campbell, P.; Green, M. A. *J. Appl. Phys.* **1987**, *62*, 243−249.
(28) Campbell, P.; Green, M. A. *Sol. Energy Mater. Sol. Cells* **2001**, *65*, 369−375.